A Conceptual Model of the Surface Salinity Distribution in the Oceanic Hadley Cell

JOHAN NILSSON AND HEINER KÖRNICH

Department of Meteorology, Stockholm University, Stockholm, Sweden

(Manuscript received 12 October 2007, in final form 11 April 2008)

ABSTRACT

A conceptual model of the salinity distribution in the oceanic Hadley cell is presented. The model pertains to the region of tropical easterly surface winds, where the surface salinity increases poleward from a local salinity minimum near the equator to a subtropical salinity maximum. A fundamental constraint is that the meridional freshwater transports in the atmosphere and the ocean have the same magnitude but opposite directions. A key assumption is that the strength of the meridional overturning cells in the atmosphere and the ocean is proportional and set by the surface layer Ekman transport. It is further assumed that, to the lowest order of approximation, the zonal-mean Ekman transports accomplish the meridional freshwater transports, that is, eddy fluxes and gyre-induced transports are ignored. The model predicts that the salinity variation in the oceanic cell is directly proportional to the specific humidity of the near-surface air, but independent of the meridional mass transport (as long as the atmospheric and oceanic mass transports remain proportional). If the relative humidity of the near-surface air is constant, the salinity variation in the oceanic Hadley cell varies essentially with the surface temperature according to the Clausius–Clapeyron expression for the saturation vapor pressure. Further, the model is compared to observations and a global warming simulation and found to give a leading-order description of the tropical surface salinity range.

1. Introduction

In the ocean, the temperature is strongly controlled by heat exchange with the atmosphere and the physical properties of seawater. For seawater, the freezing point is slightly below 0°C, setting the lower temperature limit. The warmest waters are encountered in the tropics, where strong negative feedbacks presumably have kept sea surface temperature close to 30°C throughout a considerable part of the earth's history (cf. Pierrehumbert 1995, 2002).

The oceanic salinity field appears to be less regulated than the temperature field. In the open ocean, the surface salinity varies typically between 31 and 37 g kg^{-1}; see Fig. 1. In the deep ocean, the salinity is close to 34.8 g kg^{-1}, which is essentially the mean oceanic salinity (cf. Pickard and Emery 1982). Thus, the oceanic salinity variation is not controlled by the trivial range set by pure freshwater and the very high salinity at which precipitation of salt occurs. Rather, the large-scale salinity variations are shaped by the global-scale surface freshwater flux and the oceanic circulation: The former process acts to build up salinity differences, whereas the circulation in combination with small-scale mixing acts to attenuate them. There are essentially no feedbacks between the surface salinity and the surface freshwater flux. However, the salinity affects the oceanic density field and thereby the flow field, a feature opening the possibility of multiple-equilibrium states of the ocean circulation (Stommel 1961). Thus, the salinity contrast in the ocean may well have varied significantly with the evolution of climate and continental configuration.

Figure 1 shows the zonally averaged surface salinity in the global ocean as well as the midbasin surface salinity in the Atlantic and the Pacific. These surface salinity distributions broadly reflect the pattern of evaporation minus precipitation (cf. Peixoto and Oort 1992). A general feature of the meridional surface salinity distributions is near-equatorial local minima and subtropical maxima. As shown in Fig. 1, the difference in zonally averaged surface salinity between the equatorial minimum and the subtropical maxima is roughly 1.5 g kg^{-1}. This surface salinity variation occurs in the trade

Corresponding author address: Johan Nilsson, Department of Meteorology, Stockholm University, SE-10691 Stockholm, Sweden.
E-mail: nilsson@misu.su.se

DOI: 10.1175/2008JCLI2284.1

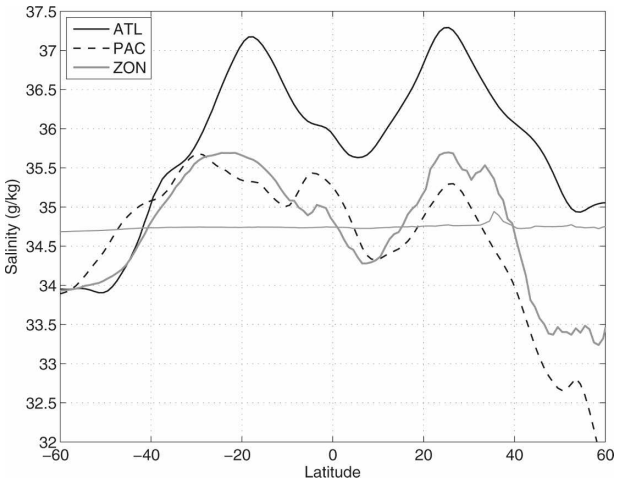

FIG. 1. Sea surface salinity in the Atlantic at 30°W (black line) and Pacific at 170°W (black dashed line). Gray lines show zonal-mean global ocean salinity distributions at the surface (thick line) and at a depth of 3500 m (thin line). In the computation of the zonal-mean salinity, values below 29 g kg^{-1} (encountered only in marginal seas) have been disregarded. The data are climatological annual-mean values taken from Antonov et al. (2006).

wind region of the Hadley cell. Here the upper-ocean waters circulate in a shallow meridional overturning cell, with poleward motion in the surface layer and equatorward motion in the upper thermocline feeding the equatorial undercurrent (see e.g., Liu 1994; McCreary and Lu 1994; Pedlosky 1996). (This circulation pattern is often called the subtropical cell; in the present paper it will also be referred to as the oceanic Hadley cell.) The water that downwells in the cell approximately conserves its surface temperature and salinity as it flows equatorward in the thermocline. Accordingly, within the cell the meridional difference in surface salinity is closely linked to the vertical salinity difference near the equator.

In this work, we present a conceptual zonally symmetric model of the salinity distribution in the oceanic Hadley cell. Although the zonal salinity variations in the tropics are comparable to the meridional ones (cf. Peixoto and Oort 1992, Fig. 8.9), we assume that the zonal-mean salinity distribution is controlled, at the lowest level of approximation, by physics that are independent of the east–west flow variations. A key physical feature, exploited in the model, is that the meridional mass transports in the Ekman layers on each side of the air–sea interface locally have the same magnitude. Held (2001) employed this equality of the Ekman mass transports to show that in the Hadley cell the partitioning of the poleward heat transport between the atmosphere and the ocean is essentially determined by the sea surface temperature distribution. Here, we will show that the equality of the Ekman mass transports couples the salinity distribution to the humidity of the near-surface air, which is essentially a function of SST if the relative humidity is fixed. This coupling is of interest in the context of climate dynamics: An increase in temperature should be associated with a stronger meridional and vertical salinity difference in the oceanic Hadley cell, which can impact on the upper-ocean flow near the equator with potential implications for the El Niño–Southern Oscillation (e.g., Fedorov et al. 2004, 2006).

In the present context, it is worth mentioning the studies of Stommel and Csanady (1980) and Ou (2007), which also consider aspects of how atmosphere–ocean interactions affect the oceanic salinity field. In contrast to the present work, these studies focus on the middle-to-high latitudes where the Ekman layer dynamics do not constrain the meridional mass transports (Czaja and Marshall 2006).

The remainder of the paper is organized as follows: The conceptual model is presented and compared to observations in section 2. In section 3, surface salinity changes associated with global warming are considered theoretically and discussed in relation to climate model simulations. The main model results are summarized and discussed in the concluding section.

2. The oceanic salinity field within the Hadley cell

Following the general approach of Held (2001), we consider an idealized model of the atmospheric and oceanic fluxes of freshwater in the Hadley cell; see Fig. 2. The model, which aims to predict the surface salinity distribution, is limited to the region with easterly surface winds and is based on the following assumptions:

1) The strength of the meridional overturning cells in the atmosphere and the ocean are proportional to each other and set by the surface Ekman mass transport;
2) the flow is steady and equatorially symmetric, implying no cross-equatorial transports;
3) the freshwater transport is accomplished by the zonal-mean advection of the zonal-mean specific humidity and salinity—that is, the freshwater transport induced by eddies and the horizontal gyre circulation is neglected;
4) the upwelling in the atmosphere and the ocean is concentrated to the equator, where all precipitation also occurs—downwelling occurs in the remainder of the cell;
5) interactions with the extratropics and the deep ocean are disregarded.

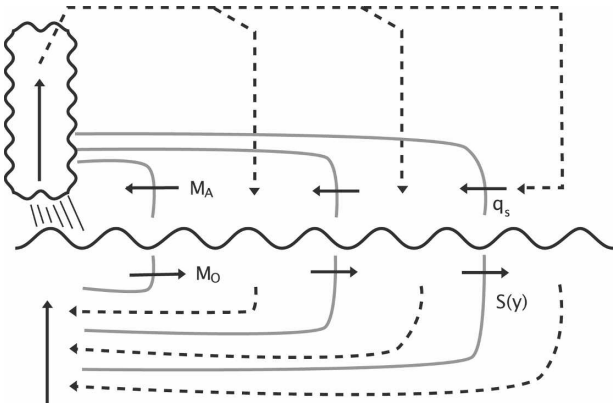

FIG. 2. A schematic of the atmosphere–ocean Hadley cell. The surface layer Ekman layer transports in the atmosphere and the ocean, denoted M_A and M_O, are of approximately equal magnitudes and set the strength of the meridional overturning cells. The gray lines in the atmosphere and the ocean illustrate isolines of specific humidity and salinity. The surface salinity $S(y)$ increases poleward, and the surface specific humidity q_s decreases poleward. See the text for details.

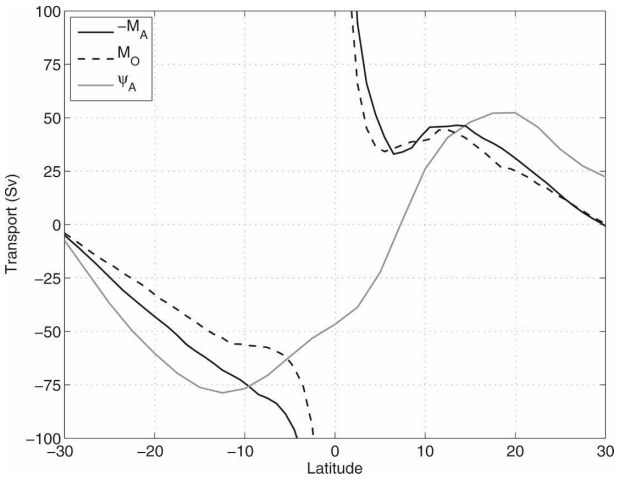

FIG. 3. Zonally integrated surface Ekman mass transport calculated from annual-mean NCEP surface wind stress (Kalnay et al. 1996). The solid line gives the (negative) atmospheric transport and the dashed line the oceanic transport; see Eqs. (1) and (2). The gray line shows the annual-mean meridional atmospheric overturning at 775 mb computed from NCEP data; positive (negative) values give the southward (northward) transport between the surface and 775 mb. The peak intensity of overturning in the annual-mean Hadley cell is encountered between 500 and 700 mb (cf. Peixoto and Oort 1992, Fig. 7.19).

Presumably, the third assumption is the most severe model restriction as transient eddies and gyre circulation give rise to freshwater fluxes that are comparable to those associated with the merdional overturning circulations (cf. Peixoto and Oort 1992; Meijers et al. 2007). Note also that the model exhibits some singular features at its boundaries: At the equator the Ekman transport becomes infinite; at the poleward edge, where the Ekman transport vanishes, the model may yield infinite salinity. These aspects of the model, which should be borne in mind, are further discussed below.

The first assumption is based on the fact that the oceanic Ekman mass transport is locally equal to and oppositefrom the atmospheric Ekman transport, which is given by τ/f, where τ is the zonal wind stress at the surface and f the Coriolis parameter (cf. Gill 1982). In the atmosphere, the net meridional mass transport in the surface Ekman layer is

$$M_A(y) = \oint \tau/f \, dx, \tag{1}$$

where x and y are zonal and meridional coordinates, respectively, and the integral extends around the globe. In the ocean, the net surface Ekman transport is

$$M_O(y) = -\int_{C_O} \tau/f \, dx, \tag{2}$$

where C_O defines the ocean-covered path along latitude circles. In the model, these expressions determine the mass transport, except very close to the equator where M_A and M_O become infinite. Figure 3 shows the meridional surface Ekman transport computed from National Centers for Environmental Prediction (NCEP) annual-mean wind stress data; also shown is the annual-mean atmospheric meridional overturning strength at 775 mb. Poleward of ~10° latitude, the surface Ekman transport gives a reasonable estimate of the annual-mean atmospheric Hadley cell transport, which reaches a peak strength of ~60 Sv (Sv $\equiv 10^6$ $m^3\ s^{-1}$, equivalently a mass transport of 10^9 kg s^{-1}); see also Peixoto and Oort (1992, Fig. 7.19). Comparable or slightly lower overturning strengths characterize the oceanic subtropical cells (cf. Bryan and Lewis 1979; Peixoto and Oort 1992, Fig. 8.20). Note that there is a geostrophic Sverdrup flow directed equatorward in parts of the oceanic cells (cf. Pedlosky 1996). Near the equator, however, the Sverdrup flow yields a surface layer transport that should be small compared to the Ekman transport (Liu 1994).

For notational convenience, we introduce

$$\xi(y) \equiv -M_A/M_O, \tag{3}$$

the ratio between the magnitudes of the meridional Ekman transports in the atmosphere and the ocean (note that $\xi > 0$ within the Hadley cell). Further, ξ^{-1} equals the fraction of the integrated zonal surface wind stress taken up by the ocean. Averaged between 30°S and 30°N, ξ^{-1} is about 0.8 for the NCEP data. From Fig. 3,

it can be inferred that a smaller fraction of the integrated zonal wind stress is generally taken up by the ocean in the Southern Hemisphere. Note further that some model results will be derived and discussed using a Northern Hemisphere perspective; these results can easily be translated to the Southern Hemisphere.

a. Freshwater and salinity fluxes

In a steady state, the zonally integrated conservation of atmospheric water can be written as

$$\frac{\partial F_A}{\partial y} = E - P, \tag{4}$$

where F_A is the net meridional transport of water and $E - P$ the zonally integrated difference between the evaporation and precipitation per unit area. Note that F_A represents the transport of water vapor as well as condensed water; however, the latter contribution is normally negligible (see Peixoto and Oort 1992, chapter 12, 273–277). The corresponding conservation of oceanic freshwater is given by

$$\frac{\partial F_O}{\partial y} = P - E. \tag{5}$$

Here F_O is the net meridional freshwater transport in the ocean and in rivers. The contribution from rivers is small in the present climate (cf. Wijffels et al. 1992) and will henceforth be neglected. It should be noted that the total meridional freshwater transport vanishes in a steady state: $F_A + F_O = 0$, showing that the oceanic and atmospheric freshwater transports have the same magnitude but opposite directions. We will denote the magnitude of the steady-state freshwater transport F.

As a first approximation, the water content in the upper troposphere is negligible compared to the near-surface water content. Thus, the equatorward water flux is set by the Ekman transport and the water mixing ratio of the air in the surface layer, which is dominated by the contribution of water vapor. These considerations imply that the atmospheric water flux is given by

$$F_A = M_A q_s, \tag{6}$$

where q_s is the specific humidity of the near-surface air. The freshwater transport predicted by this formula will be discussed in section 2b. Note that the atmospheric freshwater transport implies a net equatorward mass transport, feeding the net precipitation near the equator. As a consequence, the poleward mass transport in the upper branch of the Hadley cell is $|M_A| - F$ and the equatorward return flow in the subsurface ocean is $|M_O| - F$. However, the freshwater transport F is small compared to the Ekman transport, which follows directly from Eq. (6) since the specific humidity is much smaller than unity.

We will now use the Knudsen relation (cf. Pickard and Emery 1982, chapter 5.2, 51–54) to model the oceanic freshwater transport. In the ocean surface mixed layer, water with the salinity $S(y)$ flows poleward and becomes more saline owing to net evaporation. The equatorward return flow in the thermocline is generally distributed over a range of different salinities. We define $S_r(y)$ as the flow-weighted mean salinity of the equatorward mass flux and introduce

$$\Delta S(y) \equiv S_r(y) - S(y), \tag{7}$$

the flow-weighted salinity difference in the oceanic cell; see Eqs. (12) and (14) for formal definitions. To have a poleward oceanic freshwater flux, the return flow must be more saline than the surface water; that is, $S_r(y) > S(y)$. As the freshwater content is $1 - S$, the poleward freshwater flux is given by $M_O(1 - S)$; similarly the equatorward freshwater flux is $(M_O - F)(1 - S_r)$. The difference between these two fluxes is the net poleward oceanic freshwater flux: $F = M_O(1 - S) - (M_O - F)(1 - S_r)$. By simplifying, one obtains $F = M_O \Delta S/S_r$ (e.g., Stommel and Csanady 1980). The fact that $M_O \gg F$ implies that $S_r \gg \Delta S$, which allows S_r to be replaced by a constant mean salinity S_0. Accordingly, the oceanic freshwater flux can be written as

$$F_O = \frac{\Delta S}{S_0} M_O. \tag{8}$$

By combining Eqs. (6) and (8) and using the definition (3), we obtain the following expression for the flow-weighted salinity difference:

$$\frac{\Delta S_q}{S_0} = q_s \xi, \tag{9}$$

where the subscript q emphasizes that this is a particular expression of ΔS directly linked to the surface air specific humidity. This is the key result of the conceptual model: According to Eq. (9), the salinity difference between the water flowing equatorward and poleward, respectively, in the oceanic cell is proportional to the specific humidity of the near-surface air. Further, the reduction of the oceanic Ekman transport due to the presence of land acts to increase the salinity difference. It should be emphasized that, at the poleward cell boundary, where the meridional Ekman transport is zero, the coupling between ΔS and q_s no longer applies. Near the equator q_s reaches values of about 18×10^{-3} kg kg^{-1} (see Peixoto and Oort 1992, Fig. 12.3a), which yields $\Delta S \sim 0.6$ g kg^{-1} (using $S_0 = 35$ g kg^{-1} and $\xi = 1$).

If the relative humidity (RH) of the surface air is

fixed and the air–sea temperature difference is neglected, ΔS is given by

$$\Delta S_q = S_0(\mathrm{RH} q_*(T_s))\xi, \tag{10}$$

where T_s is the SST and q_* the saturation specific humidity. This implies that the vertical salinity difference in the oceanic Hadley cell is essentially a function of the SST.

It should be recalled that ΔS is the difference between the flow-weighted subsurface salinity S_r and the surface salinity. Under the assumptions of the present model, ΔS can be calculated from the surface salinity and the Ekman transport if the turbulent diffusive salinity flux at the base of the mixed layer is negligible.[1] In this case, the salinity flux from the mixed layer into thermocline is purely advective and locally given by

$$-S(y)\frac{dM_O}{dy}\,dy. \tag{11}$$

The salinity flux carried by the equatorward flow in the thermocline at latitude y is obtained by integrating this expression to the poleward cell boundary at $y = y_P$:

$$S_r \cdot M_O = -\int_y^{y_P} S\frac{dM_O}{dy'}\,dy'. \tag{12}$$

This expression defines $S_r(y)$, the flow-weighted mean salinity of the equatorward flow. Integrating by parts and using the fact that M_O is zero at the poleward cell boundary, one obtains

$$\Delta S M_O = \int_y^{y_P} M_O\frac{dS}{dy'}\,dy', \tag{13}$$

where the definition $\Delta S = S_r(y) - S(y)$ has been used. Thus, by neglecting horizontal gyre and eddy transport as well as the vertical diffusive flux, the vertical salinity difference ΔS is given by

$$\Delta S_M = \frac{1}{M_O}\int_y^{y_P} M_O\frac{dS}{dy'}\,dy', \tag{14}$$

where the subscript M distinguishes this particular estimate of ΔS. To illustrate some basic features of this formula, we consider a simple case with a constant surface salinity gradient and an Ekman profile of the form $M_O \propto (1 - y/y_P)^b$, where $b \geq 0$ controls the shape of M_O. In this case, Eq. (14) yields

$$\Delta S(y) = \frac{(1 - y/y_P)}{1 + b}\,y_P\frac{dS}{dy}, \tag{15}$$

where $y_P dS/dy$ is the surface salinity range. For uniform downwelling, corresponding to $b = 1$, the maximum ΔS is one-half of the surface salinity range. This linear M_O profile gives a reasonable description of the Ekman transport poleward of 10°. For b smaller (larger) than unity the downwelling becomes concentrated toward the equatorward (poleward) cell boundary, yielding larger (smaller) values of ΔS. If all downwelling occur at the poleward cell boundary, corresponding to $b = 0$, ΔS equals the full surface salinity range.

b. *The model ΔS and freshwater transport computed from observations*

The relations (9) and (14) give two independent ways of calculating the flow-weighted vertical salinity difference ΔS. The former relation, connecting the salinity with the surface specific humidity, arises from the constraint that the oceanic and atmospheric freshwater transports are equal and given by Eqs. (4) and (5), respectively. The latter relation specifies ΔS in terms of the surface salinity and the Ekman transport. This relation, pertaining to the state of the ocean, does not involve any assumptions on the atmospheric freshwater transport. If the model assumptions are correct, these two formulas should give the same results. To examine this, we use NCEP data of surface specific humidity and wind stress (Kalnay et al. 1996) and surface salinity data (Antonov et al. 2006) to calculate ΔS_q and ΔS_M. Figure 4 shows the results, which are based on time-mean zonally averaged observations.

The ΔS_q estimate yields near-equatorial values in the range 0.6–0.8 g kg^{-1}. The higher value is obtained when accounting for the fact that ξ tends to be greater than unity; see Eq. (3). As discussed in connection with Eq. (15), the near-equatorial ΔS_q values are essentially compatible with the scenario in which the water in the oceanic Hadley cell subducts and moves equatorward, conserving its surface salinity signature. Comparable maximum values of ΔS_M are obtained when observed surface salinity and Ekman transport are used in Eq. (14). However, the two methods for calculating ΔS yield results that differ qualitative in some notable aspects. In particular, ΔS_q is larger near the poleward cell boundary than ΔS_M. It is illuminating to consider the meridional derivative of ΔS_M, which using Eq. (14) can be written as

$$\frac{d\Delta S_M}{dy} = -\frac{dM_O}{dy}\frac{\Delta S_M}{M_O} - \frac{dS}{dy}. \tag{16}$$

[1] Klinger and Marotzke (2000) and Held (2001) used a similar approach to estimate the effective temperature difference of the water flowing in the oceanic Hadley cell.

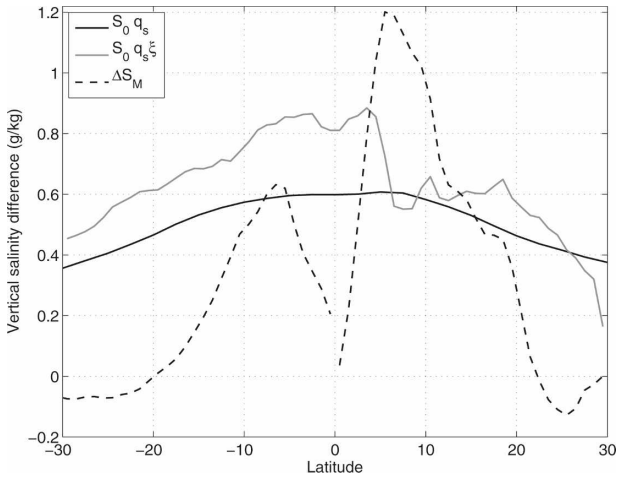

FIG. 4. Estimates of the flow-weighted salinity difference ΔS, defined by Eq. (7), based on annual-mean zonally averaged observations. The black and the gray line show $S_0 q_s \xi$ and $S_0 q_s$, respectively, based on zonal surface wind stress and surface specific humidity from NCEP (Kalnay et al. 1996); see Eq. (9). The dashed line shows ΔS_M, defined by Eq. (14), calculated from NCEP surface wind stress and *World Ocean Atlas* surface salinity (Antonov et al. 2006).

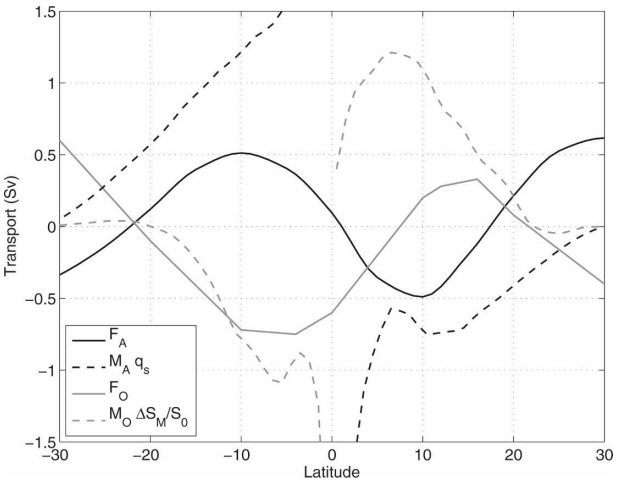

FIG. 5. Meridional freshwater transport in the atmosphere (black lines) and ocean (gray lines). Here F_A is based on $E - P$ data (Peixoto and Oort 1992, Table 12.1) and F_O is taken from Wijffels et al. (1992). The atmospheric estimate $M_A q_s$ (black dashed) is computed using the zonally averaged surface specific humidity and surface wind stress from NCEP (Kalnay et al. 1996). The oceanic estimate $M_O \Delta S_M / S_0$ (gray dashed) is computed using zonally averaged NCEP wind stress and zonally averaged surface salinity from the *World Ocean Atlas* (Antonov et al. 2006).

Due to the poleward decrease of the Ekman transport, the first term is generally positive. Accordingly, the poleward decrease of ΔS_M is primarily controlled by the poleward increase of the zonal-mean surface salinity. In particular, the high Northern Hemisphere ΔS_M values reflect the strong surface salinity gradient between 10° and 25°N, and the near-equatorial drop in ΔS_M reflects the strong equatorward increase of M_O. Near the poleward cell boundaries, where the surface salinity decreases poleward, ΔS_M becomes negative.

To examine why the two methods for calculating ΔS give different results, we compute the implied freshwater transports and compare these with independent information on the meridional freshwater transport. Figure 5 shows the estimates $F_A = M_A q_s$ and $F_O = M_O \Delta S_M / S_0$, calculated using zonally averaged time-mean observations of surface wind stress, specific humidity, and salinity; see Eqs. (4), (5), and (14). It is helpful to note that $-F_O/F_A = \Delta S_M / \Delta S_q$. Thus, it can be directly inferred from Fig. 4 that, in the Southern Hemisphere where $\Delta S_q > \Delta S_M$, the freshwater transport estimate in the atmosphere exceeds that in the ocean. The simple formulas yield results that are in broad agreement with the independent freshwater transport estimates shown in Fig. 5, namely, the F_O estimate of Wijffels et al. (1992) and the F_A estimate based on the $E - P$ data in Table 12.1 in Peixoto and Oort (1992). In fact, at 10° latitude the present simple estimates are essentially within the range of transports reported in the literature (cf. Beranger et al. 1999). Near the equator and the poleward cell boundary, the simple formulas perform worse.

It should be emphasized that the simple formulas Eqs. (4) and (5) give estimates only of the freshwater transport contribution owing to the time-mean zonally averaged overturning circulation. Obviously, the present Ekman-layer-based estimates of this transport contribution are not perfect. They fail near the equator and the use of the surface specific humidity in Eq. (4) should overestimate the atmospheric freshwater transport. The equatorward-flowing branch of the Hadley cell reaches up above 700 mb, and over this height range the specific humidity decreases by about a factor of 2. Furthermore, the poleward transient eddy moisture transport is important near the poleward edge of the atmospheric Hadley cell (see Peixoto and Oort 1992, Fig. 12.12). The absence of the transient eddy transport in the estimate $M_A q_s$ yields a freshwater transport that changes sign near 30° latitude, rather than near 20° latitude as suggested by observations. In the near-equatorial ocean, the time-mean horizontal gyre circulation tends to produce equatorward transports of freshwater and heat comparable to that produced by the overturning circulation, whereas the transient eddy transports tend to be small (see e.g., Hazeleger et al. 2004; Meijers et al. 2007). Thus, the neglect of the gyre-induced oceanic freshwater trans-

port should make the estimate $F_O = M_O \Delta S_M / S_0$ too large near the equator, where furthermore the Ekman transport overestimates the overturning circulation.

In summary, the Eqs. (4) and (5) represent estimates of the freshwater transport component that results from the advection of the zonal-mean surface humidity and salinity fields by the time-mean meridional overturning circulations. These simple estimates give the order of magnitude of the freshwater transport in the central Hadley cell. However, the presence of additional freshwater transport due to transient eddies and gyre circulation, which affect the distributions of humidity and salinity, causes the two simple estimates to differ. As a result, the assumed correspondence between ΔS_q and ΔS_M is only qualitative; see Fig. 4.

c. The surface salinity distribution

We now demonstrate that the model assumptions also entail an equation for the surface salinity distribution, which can be derived as follows: Starting from Eq. (5) and writing the oceanic freshwater transport as $F_O = M_O \Delta S_M / S_0$ [see Eq. (14)], after straightforward manipulations we obtain

$$\frac{M_O}{S_0}\frac{dS}{dy} = E - P. \tag{17}$$

It should be noted that this formula is singular at the equator if M_O becomes infinite there. Further, it is generally a singular poleward cell boundary; see the comment below.

The physical content of Eq. (17) is simple: In the mixed layer, the salinity tendency due to the zonally integrated surface freshwater flux, taken be positive in the model domain, balances the advective tendency; that is, the salinity of the surface water parcels increase as they move poleward. Two additional features of Eq. (17) deserve to be pointed out. First, it depends only on the physics in the mixed layer; that is, it is valid independently of whether the salinity is materially conserved in the thermocline as long as the diffusive salinity flux at the base of the mixed layer is negligible. Second, the relation will predict infinite salinity gradients at the poleward cell boundary (where M_O is assumed to vanish) for nonzero $E - P$. Here, neglected physics such as eddy-induced mixing and geostrophic gyre circulation accomplish the oceanic freshwater convergence necessary to balance $E - P$. In the real ocean, these neglected processes act to limit the surface salinity near the poleward cell boundary.

By rewriting $E - P$ using the Eqs. (4) and (6), Eq. (17) yields

$$\frac{M_O}{S_0}\frac{dS}{dy} = \frac{d(q_s M_A)}{dy}. \tag{18}$$

Further, by using the definition $M_A = -M_O \xi$ [see Eq. (3)], expanding the term on the right-hand side, and dividing with M_O, after straightforward manipulations one obtains

$$\frac{1}{S_0}\frac{dS}{dy} = -\frac{d(q_s \xi)}{dy} - \frac{q_s \xi}{M_O}\frac{dM_O}{dy}. \tag{19}$$

Finally, by using Eq. (9), this can be rewritten as

$$\frac{dS}{dy} = -\frac{d\Delta S_q}{dy} - \frac{\Delta S_q}{M_O}\frac{dM_O}{dy}, \tag{20}$$

which is analogous to Eq. (16). Given M_A, M_O, and q_s, the surface salinity distribution can be calculated from the equivalent Eqs. (18)–(20). According to these equations, the poleward increase of the surface salinity is essentially controlled by the rate at which the distributions of the surface specific humidity and the Ekman transport decline poleward.

Some basic properties of Eq. (19) can be illustrated by calculating a hypothetical salinity distribution based on idealized distributions of M_O and q_s. For convenience we introduce a scaled coordinate y, which is zero at the equator and unity at the poleward edge of the Hadley cell. We use the humidity profile $q_s(y) = q_e - \Delta q y^2$, which gives a rough fit to the observed zonal-mean q_s (see Fig. 4), and the Ekman profile used in connection with Eq. (15); that is, $M_O \propto (1 - y)^b$. Solving Eq. (19) with $\xi = 1$, one obtains

$$S(y) - S(0) = S_0\{\Delta q y^2 + b[\Delta q(y^2/2 + y) - (q_e - \Delta_q)\ln(1 - y)]\}. \tag{21}$$

This expression diverges at the poleward edge of the Hadley cell where the Ekman transport vanishes. However, the logarithmic singularity influences the solution only close to the poleward cell boundary. In the limiting case $b = 0$, M_O is constant, which implies that all downwelling occurs at the poleward cell boundary. In this case, Eq. (21) reduces to $S(y) - S(0) = S_0 \Delta q y^2$, which defines a minimum salinity gradient. Below, the cases $b = 0$ and $b = 1$ will be discussed in relation to the observed surface salinity distribution.

We now calculate the surface salinity field defined by Eq. (19) using zonally-averaged time-mean surface specific humidity and wind stress data (Kalnay et al. 1996). In each hemisphere, Eq. (19) is integrated poleward from 0.5° to near 30° latitude; the arbitrary integration constants are then adjusted to match the observed salinity field. In addition, we have extracted the equato-

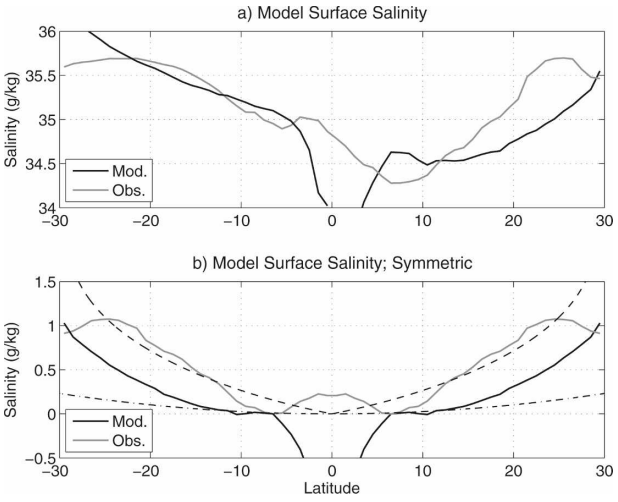

FIG. 6. (a) The model surface salinity distribution (black lines), defined by Eq. (20), and the observed zonal-mean surface salinity (gray lines). The model salinity is computed from the zonal-mean NCEP surface specific humidity and zonal wind stress; see the text for details. (b) The equatorially symmetric components of the salinity distributions in (a) with a reference salinity subtracted; also, analytical salinity profiles defined by Eq. (21) are illustrated: the dashed (dashed–dotted) lines represent $b = 1$ ($b = 0$); the values $q_e = 17.2$ and $\Delta q = 6.6$ g kg^{-1} are used, which approximate the equatorially symmetric surface humidity field.

rially symmetric components of the model salinity and the observed salinity. Figure 6 shows the results. Equatorward of about 5°, Eq. (19) yields salinity distributions with unrealistically large gradients. This is caused by the large near-equatorial amplitudes of M_O, which overestimates the real poleward transport in the surface layer. In the latitude band between 10° and 20°, roughly, the model-calculated salinity gradients are in broad agreement with the observed ones. Here, the model gives a slightly better fit to the observations in the Southern Hemisphere (and in the equatorially symmetric picture) than in the Northern Hemisphere. It can be noted that the analytical profile defined by Eq. (21), with $b = 1$ and humidity values based on observations, gives a fair description of the observed symmetric salinity gradient in the central cell.

Near 5° latitude, M_O has a weaker poleward gradient (see Fig. 3). Here, the second term on the rhs of Eq. (19) is small, and the model salinity gradient is set by the poleward decline of the near-surface specific humidity field. Consequently, the analytical profile (21) with $b = 0$ gives a decent description of the symmetric salinity gradient in this region. Near the poleward cell boundary, where M_O becomes insignificant for the freshwater transport in the real ocean, the model fails to capture the reduction and eventual sign reversal of the observed surface salinity gradient.

3. Climate change and variations of the tropical surface salinity

a. *Scaling and temperature dependence of the salinity field*

The present model of the oceanic Hadley cell predicts that the flow-weighted salinity difference ΔS is proportional to the specific humidity of the surface air; see Eq. (9). An important consequence is that, if the near-surface relative humidity is invariant, then ΔS will essentially increase with temperature according to the Clausius–Clapeyron (CC) expression for the saturation vapor pressure

$$\frac{d \ln e_*}{dT} = \frac{L}{RT^2} \equiv \alpha(T), \tag{22}$$

where e_* is the saturation vapor pressure, L the latent heat of vaporization, and R the gas constant; for typical surface temperatures $\alpha \approx 0.07$ K^{-1} (cf. Gill 1982). Also, for present-day atmospheric temperatures the temperature dependence of the saturation specific humidity follows Eq. (22) approximately (cf. Emanuel 1994, chapter 4.1, 107–109); that is,

$$\frac{d \ln q_*}{dT} \approx \alpha(T).$$

From Eq. (9) it follows that, for small changes δq_s and $\delta\xi$, the resulting change of ΔS is $\delta \Delta S \approx S_0(\xi \delta q_s + q_s \delta\xi)$. Thus, the relative change of ΔS is given by

$$\frac{\delta \Delta S}{\Delta S} \approx \frac{\delta q_s}{q_s} + \frac{\delta \xi}{\xi}. \tag{23}$$

In what follows, we consider the salinity response to an essentially uniform warming of the tropical sea and air surface temperature. Further, we assume that the surface relative humidity is fixed, implying that $\delta q_s / q_s \approx \alpha \delta T$ and that the temperature-related relative change of the specific humidity is much larger the relative change of the Ekman transports; that is, $\alpha \delta T \gg \delta\xi/\xi$. In this case, Eq. (23) simplifies to

$$\frac{\delta \Delta S}{\Delta S} \approx \alpha \delta T, \tag{24}$$

showing that a 1° temperature increase entails a ΔS increase of about 7%. Note that the change of ξ will be small as long as the Ekman mass transports in the atmosphere and the ocean remain roughly proportional, even if the amplitude of the transports change; see Eq. (3).

Furthermore, if the shape of M_O is invariant, then the changes of the meridional surface salinity gradient will

approximately mirror the changes of ΔS. A scaling analysis of Eq. (20) shows that the first term on the right-hand side (proportional to the horizontal variation of ΔS) is generally small compared to the second term (proportional to ΔS since the variation of M_O is comparable to its amplitude). Thus, the relative change of the meridional surface salinity gradient is approximately given by

$$\frac{\delta(dS/dy)}{dS/dy} \approx \frac{\delta \Delta S}{\Delta S}.$$

As a result, the changes of the horizontal surface salinity variation will approximately follow the CC scaling:

$$\delta[S(y) - S(y_1)] \approx \alpha \delta T[S(y) - S(y_1)], \qquad (25)$$

where $S(y_1)$ is an arbitrary integration constant. This expression suggests that the shape of the tropical surface salinity field is approximately invariant under uniform changes of sea surface temperature, provided that the form of M_O is preserved. It is relevant to point out that also the atmospheric meridional freshwater transport obeys approximately the CC scaling when the specific humidity changes dominate over the changes in mass transport (cf. Held and Soden 2006):

$$\frac{\delta F}{F} \approx \frac{\delta q_*}{q_*} \approx \alpha \delta T. \qquad (26)$$

b. *Salinity changes in a climate model simulation of global warming*

As an illustration of how the surface salinity may respond to climate change, we have analyzed a climate model simulation of CO_2-induced global warming. Here we have taken results from the "1% yr^{-1} CO_2 increase experiment (to doubling)" with the ECHAM5/MPI-OM,[2] check deleted footnotewhich starts from preindustrial conditions and attains doubling of CO_2 after 70 years. Then the model integration continues at this CO_2 level. Figure 7 shows the zonal-mean sea surface temperature and salinity averaged over two 10-yr periods: one starting the model year 1860 at the beginning of the experiment and the other from the model year 2070 at the end of the simulation. The increase in tropical SST at the end of the integration is about 3 K. The shape of the simulated zonally averaged surface salinity fields are in broad agreement with the observations shown in Fig. 1. One difference, however, is that

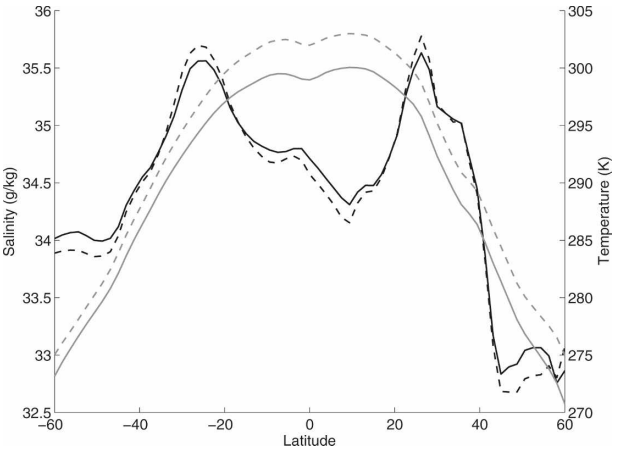

FIG. 7. Zonally averaged sea surface salinity (black) and temperature (gray) from the "1% yr^{-1} CO_2 increase (to doubling)" with the ECHAM5/MPI-OM. Solid and dashed lines refer to a 10-yr mean over model years 1860–69 and 2070–79, respectively. Salinity values below 29 g kg^{-1} have been omitted in the calculation of the zonal average.

the simulated subtropical salinity maxima are more pointed than the observed ones. It should be noted that the salinity field, particularly in the deep ocean, is not in equilibrium in this transient simulation. However, the surface salinity in the oceanic Hadley cell should be sufficiently close to equilibrium to make a qualitative comparison with our conceptual steady-state model relevant. Calculations of ΔS_q and ΔS_M from the model output (not shown) yield results that are broadly similar to the observationally based calculations shown in Fig. 4; for example, also in the simulation, ΔS_M reaches higher values in the Northern Hemisphere cell. Figure 8 shows the ECHAM5/MPI-OM freshwater transport for model years 1860–69 as well as the freshwater transport estimates calculated from Eqs. (4) and (5). In the Southern Hemisphere, the simple formulas give a good description of the freshwater transports in the central part of the cell. In the Northern Hemisphere, where the ECHAM5/MPI-OM yields a weak freshwater transport, the simple formulas overestimate the transports. This suggests that, in the ECHAM5/MPI-OM, the freshwater transports owing to transient eddy fluxes and oceanic gyre circulation are stronger in the Northern Hemisphere than in the Southern Hemisphere.

Figure 9 shows the relative changes of the zonal-mean surface specific humidity and the parameter ξ as well as the CC-scaled temperature change $\alpha \delta T$. It can be noted that the relative humidity is slightly decreased as the model warms, causing the CC scaling to overestimate the surface humidity change. As a first approximation, however, the surface specific humidity follows

[2] The results are obtained from the World Climate Research Programme's (WCRP's) Coupled Model Intercomparison Project phase 3 (CMIP3) multimodel dataset.

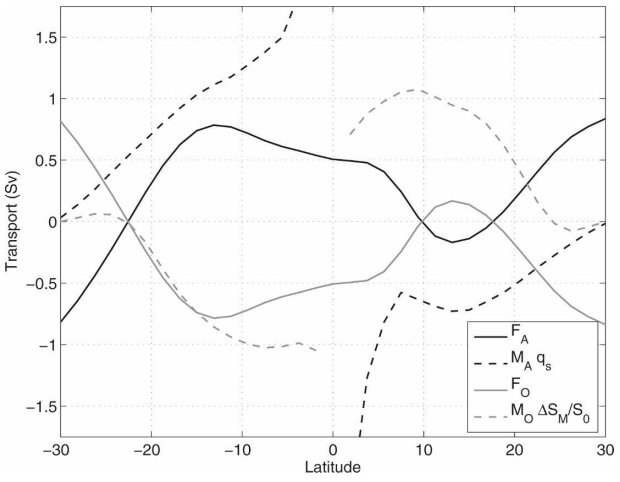

FIG. 8. Meridional freshwater transport in the atmosphere (black lines) and in the ocean (gray lines) in the ECHAM5/MPI-OM simulation the years 1860–69. Here F_A is based on the $E - P$ field and $F_O = -F_A$. The atmospheric estimate $M_A q_s$ (black dashed) and oceanic estimate $M_O \Delta S_M / S_0$ (gray dashed) are computed using the zonally averaged surface specific humidity and surface wind stress; see Eqs. (4), (5), and (14). The structure of these curves is roughly invariant as the model warms and their amplitudes follow approximately the CC scaling.

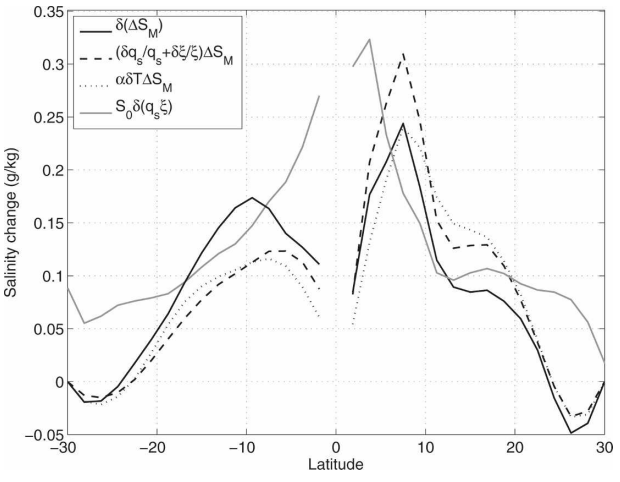

FIG. 10. Change in the flow-weighted salinity difference ΔS in the ECHAM5/MPI-OM simulation. The solid black and gray lines are the difference between the 10-yr means of ΔS_M and ΔS_q, respectively, from the model years 2070–79 and 1860–69. The dashed and the dotted lines are $(\delta q_s/q_s + \delta\xi/\xi)\Delta S_M$ and $\alpha\delta T \Delta S_M$, where ΔS_M is taken from the years 1860–69. The factor $\delta q_s/q_s + \delta\xi/\xi$ is computed as described in Fig. 9, and $\alpha\delta T = 0.2$, which is an approximation based on the mean tropical (30°S–30°N) temperature increase.

the CC scaling. In the Hadley cell, the warming entails some slight changes of the zonal surface wind stress and, hence, the meridional Ekman transport. Between 10°S and 10°N ξ increases, reflecting a decrease of the fraction of the integrated zonal wind stress that is taken up by the ocean. However, the relative changes of ξ are generally negligible compared to $\alpha\delta T$. Further, the changes of the atmospheric freshwater transport (not shown) roughly follow the CC scaling; see Eq. (26) and the discussion in Held and Soden (2006).

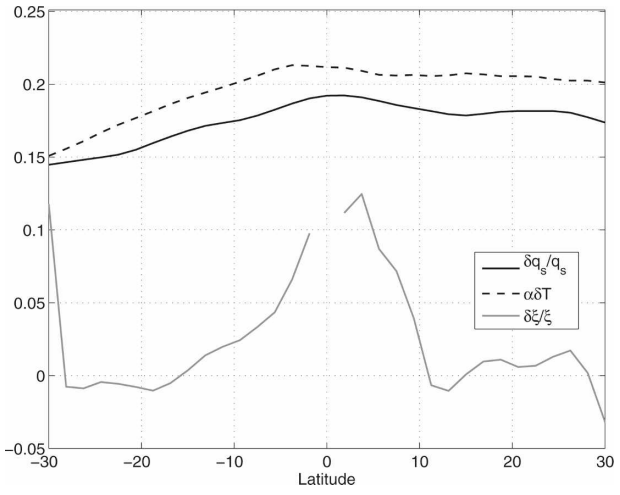

FIG. 9. Relative change of the surface specific humidity (black solid line) and the parameter ξ (gray solid line) in the ECHAM5/MPI-OM simulation. The changes are computed as $[q_s(t_2) - q_s(t_1)]/q_s(t_1)$ and $[\xi(t_2) - \xi(t_1)]/\xi(t_1)$, where t_1 and t_2 denote mean values from the model years 1860–69 and 2070–79, respectively. The dashed line is the Clausius–Clapeyron implied change, computed from the surface air temperature as $\alpha[T_s(t_2) - T_s(t_1)]$. Note that near-equatorial increase of ξ implies that the oceanic Ekman transport is reduced relative to the atmospheric one; see Eq. (3).

We now examine the changes of ΔS in the model, which according to Eq. (24) should approximately follow the CC scaling. Figure 10 shows the difference in ΔS_M and ΔS_q between model years 2070–79 and 1860–69. In addition, the figure shows $\Delta S_M(y)$, taken from the model years 1860–69, multiplied with 0.2 and the quantity $(\delta q_s/q_s + \delta\xi/\xi)$; see Fig. 9. The factor 0.2 is based on the CC scaling $\alpha\delta T$ using $\delta T = 3$ K. It is evident that the CC scaling gives a reasonable approximation of the ΔS_M changes associated with the warming. The more accurate relation given by Eq. (23), which does not assume fixed relative humidity and accounts for the changes of ξ, is in practice indistinguishable from the CC scaling. It can further be noted that the change of ΔS_q gives an order of magnitude prediction of the ΔS_M change.

Figure 11 shows the zonal-mean surface salinity change between the model years 2070–79 and 1860–69. In the subtropics, the surface salinity increases; elsewhere, it decreases. Roughly, the surface salinity increases in the latitude bands where the zonal-mean $E - P$ is positive. Also shown is the CC prediction of the

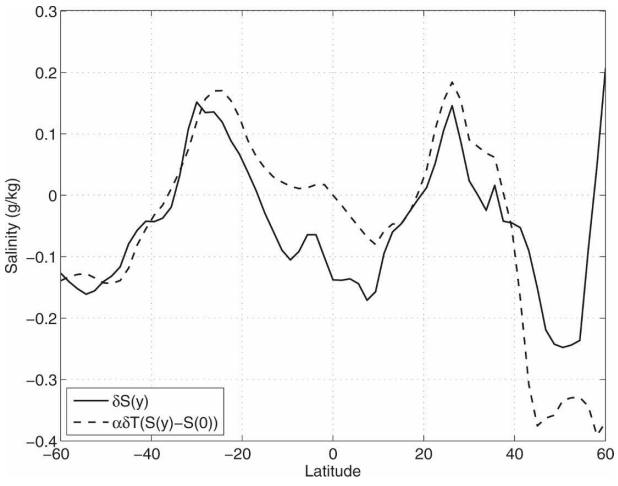

FIG. 11. Change in surface salinity distribution in the ECHAM5/MPI-OM simulation. The solid line is the difference between the 10-yr salinity means from 2070–79 and 1860–69. The dashed line is the salinity variation, defined as $S(y) - S(y = 0)$, from the years 1860–69 multiplied with the Clausius–Clapeyron scaling $\alpha\delta T$, i.e., $\alpha\delta T[S(y) - S(y = 0)]$. Here $\alpha\delta T = 0.2$ based on the mean tropical 30°S–30°N temperature increase.

surface salinity change given by Eq. (25). This quantity is obtained by multiplying the surface salinity variation, defined as $S(y) - S(0)$, from the model years 1860–69 with $\alpha\delta T$, which is taken as 0.2. Note that the choice of the reference salinity $S(0)$ is arbitrary; that is, the CC scaling cannot predict the absolute salinity change. Thus, it is only the form and the range of the two salinity profiles in Fig. 11 that should be compared. In the tropics, there is a qualitative agreement between the CC-predicted salinity change and the climate model response. However, the CC scaling underestimates the change of the salinity difference between the near-equatorial minimum and the subtropical maximum: the CC-predicted change is about 0.25 g kg^{-1}; whereas, the simulation yields a change of 0.32 g kg^{-1}. Around 20° latitude the CC scaling gives a good description of the change of the surface salinity gradient. Note that the latitude band where this applies is wider in the Northern Hemisphere where the CC scaling captures the salinity gradient change between about 10° and 25°N. It should be recalled that Eq. (25) requires that the shape of M_O is invariant. Thus, structural changes of the Ekman transport near the equator, hinted in Fig. 9, may contribute to the poorer performance of the CC scaling in that area, where furthermore the validity of the conceptual model breaks down. The correspondence between the CC scaling and the simulated salinity change between 30° and 50°S is striking. A brief inspection of few other CMIP3 models suggests that this is not a universal model response to CO_2-induced global warming. However, the surface salinity response should roughly follow the CC scaling, if the $E - P$ pattern does, and the changes of the ocean currents can be neglected.

4. Discussion

A conceptual model of the salinity field in the oceanic Hadley cell has been presented. The model makes several simplifying assumptions and furthermore lacks the physics necessary to fully describe the freshwater transport and the salinity field near the equator and the poleward cell boundary. Thus, the model serves to illuminate the physics that shape the tropical surface salinity field, but its predictions will be of qualitative nature.

The main model result is that the salinity difference between the water flowing poleward in the surface layer and equatorward in the thermocline should be proportional to the specific humidity of the surface air, but essentially independent of the cell mass transport; see Eq. (9). This vertical flow-weighted salinity difference ΔS, which reinforces the thermal density stratification, is largest near the equator where it is comparable to (but less than) the meridional surface salinity difference over the cell. Using observed near-equatorial surface humidity and surface wind stress, Eq. (9) yields $\Delta S \sim 0.8$ g kg^{-1}, a value consistent with the observed surface salinity range in the oceanic Hadley cell; see Figs. 1 and 4. Also Eq. (14), which specifies ΔS in terms of the surface salinity and the oceanic Ekman transport, gives results of a comparable magnitude. If the model accurately described the oceanic and atmospheric freshwater transports, then the data-based calculations of ΔS_q and ΔS_M would give identical results. As illustrated in Fig. 5, however, the model is only capable of predicting the order of magnitude of the freshwater transport in the central part of the Hadley cell. In this region, the simple model of the surface salinity field given by Eq. (20) has some skill in predicting the observed surface salinity gradient; see Fig. 6.

An important implication of the model concerns climate change. If the relative humidity of the near-surface air is constant, the salinity range in the oceanic Hadley cell is predicted to vary with the sea surface temperature according to the Clausius–Clapeyron expression for the saturation vapor pressure: for example, an ~3°C cooling of the equatorial sea surface temperature during the last glacial maximum (Lea et al. 2000) should have entailed a 20% reduction of the surface salinity variation from the equator to the subtropics. The analyses of the ECHAM5/MPI-OM simulation re-

ported here show that the CC scaling provides a useful prediction of the tropical surface salinity response to the CO_2-induced global warming in that model; see Figs. 10 and 11. It should be emphasized that we have presented results from a single climate-model simulation, implying that the salinity change illustrated in Fig. 11 could be model dependent. We have inspected the changes of the surface salinity in a few other global warming simulations in the Program for Climate Model Diagnosis and Intercomparison archive. In the extratropics, there are qualitative intermodel differences in the response of the surface salinity field (i.e., the good agreement between the CC scaling and the surface salinity change in the Southern Hemisphere midlatitudes displayed in Fig. 11 is not a general feature). Within the Hadley cell, on the other hand, the simulated changes of the surface salinity range tend to approximately follow the Clausius–Clapeyron scaling.

In the extratropics, where baroclinic eddies and deep meridional oceanic overturning are important freshwater transport agents, the coupling between the surface humidity and salinity may be weak, implying that the CC scaling does not necessarily constrain the changes of the zonal-mean surface salinity. Here, the atmospheric and oceanic mass transports are not coupled by the Ekman layer dynamics (see e.g., Czaja and Marshall 2006) and, hence, may exhibit different responses to a climate change. In particular, feedbacks between the salinity field and the deep meridional overturning (cf. Walin 1985; Bryan 1986; Rahmstorf 1996; Nilsson and Walin 2001; Dijkstra and Weijer 2005) can induce pronounced reorganizations of the high-latitude upper-ocean salinity field—a fact that may contribute to the intermodel differences of the extratropical surface salinity response. Thus, a relevant extension of the present work would be a more thorough analysis of the salinity response in the CMIP3 dataset.

Acknowledgments. We thank R. Caballero, R. T. Pierrehumbert, and G. Walin for comments and discussions. We also thank two anonymous reviewers for their insightful comments and suggestions, which improved the presentation. The work reported here was supported by the Swedish Research Council and is a contribution from the Bert Bolin Climate Research Centre at Stockholm University. We acknowledge the modeling groups, the Program for Climate Model Diagnosis and Intercomparison (PCMDI) and the WCRP's Working Group on Coupled Modelling (WGCM) for their roles in making the WCRP CMIP3 multimodel dataset available. Support of this dataset is provided by the Office of Science, U.S. Department of Energy.

REFERENCES

Antonov, J. I., R. A. Locarnini, T. P. Boyer, A. V. Mishonov, and H. E. Garcia, 2006: *Salinity.* Vol. 2, *World Ocean Atlas 2005,* NOAA Atlas NESDIS 62, 182 pp.

Beranger, K., L. Siefridt, B. Barnier, E. Garrnier, and H. Roquet, 1999: Evaluation of operational ECMWF surface freshwater fluxes over oceans during 1991–1997. *J. Mar. Syst.,* **22,** 477–493.

Bryan, F., 1986: High-latitude salinity effects and interhemispheric thermohaline circulations. *Nature,* **323,** 301–323.

Bryan, K., and L. J. Lewis, 1979: A water mass model of the world ocean. *J. Geophys. Res.,* **84,** 2503–2517.

Czaja, A., and J. Marshall, 2006: The partitioning of poleward heat transport between the atmosphere and ocean. *J. Atmos. Sci.,* **63,** 1498–1511.

Dijkstra, H. A., and W. Weijer, 2005: Stability of the global ocean circulation: Basic bifurcation diagrams. *J. Phys. Oceanogr.,* **35,** 933–948.

Emanuel, K. A., 1994: *Atmospheric Convection*. 1st ed. Oxford University Press, 580 pp.

Fedorov, A. V., R. C. Pacanowski, S. G. Philander, and G. Boccaletti, 2004: The effect on salinity on the wind-driven circulation and the thermal structure of the upper ocean. *J. Phys. Oceanogr.,* **34,** 1949–1966.

——, P. S. Dekens, M. McCarthy, A. C. Ravelo, P. B. deMenocal, M. Barreiro, R. C. Pacanowski, and S. G. Philander, 2006: The pliocene paradox (mechanisms for a permanent El Niño). *Science,* **312,** 1485–1489.

Gill, A. E., 1982: *Atmosphere–Ocean Dynamics*. 1st ed. Academic Press, 662 pp.

Hazeleger, W., R. Seager, M. A. Cane, and N. H. Naik, 2004: How can tropical Pacific Ocean heat transport vary? *J. Phys. Oceanogr.,* **34,** 320–333.

Held, I. M., 2001: The partitioning of the poleward energy transport between the tropical ocean and atmosphere. *J. Atmos. Sci.,* **58,** 943–948.

——, and B. J. Soden, 2006: Robust response of the hydrological cycle to global warming. *J. Climate,* **19,** 5686–5699.

Kalnay, E., and Coauthors, 1996: The NCEP/NCAR 40-Year Reanalysis Project. *Bull. Amer. Meteor. Soc.,* **77,** 437–471.

Klinger, B. A., and J. Marotzke, 2000: Meridional heat transport by the subtropical cell. *J. Phys. Oceanogr.,* **30,** 696–705.

Lea, D. W., D. K. Pak, and H. J. Spero, 2000: Climate impact of late quaternary equatorial Pacific sea surface temperature variations. *Science,* **289,** 1719–1724.

Liu, Z., 1994: A simple model of the mass exchange between the subtropical and tropical ocean. *J. Phys. Oceanogr.,* **24,** 1153–1165.

McCreary, J. P., and P. Lu, 1994: Interaction between the subtropical and equatorial ocean circulations: The subtropical cell. *J. Phys. Oceanogr.,* **24,** 466–497.

Meijers, A. J., N. L. Bindoff, and J. L. Roberts, 2007: On the total, mean, and eddy heat and freshwater transport in the Southern Hemisphere of a $\frac{1}{8}^\circ \times \frac{1}{8}^\circ$ global ocean model. *J. Phys. Oceanogr.,* **37,** 277–295.

Nilsson, J., and G. Walin, 2001: Freshwater forcing as a booster of thermohaline circulation. *Tellus,* **53A,** 629–641.

Ou, H. W., 2007: Hydrological cycle and ocean stratification in a coupled climate system: A theoretical study. *Tellus,* **59A,** 683–694.

Pedlosky, J., 1996: *Ocean Circulation Theory*. 1st ed. Springer-Verlag, 453 pp.

Peixoto, J. P., and A. H. Oort, 1992: *Physics of Climate*. American Institute of Physics, 520 pp.

Pickard, G. L., and W. J. Emery, 1982: *Descriptive Physical Oceanography*. 4th ed. Pergamon, 249 pp.

Pierrehumbert, R. T., 1995: Thermostats, radiator fins, and the local runaway greenhouse. *J. Atmos. Sci.,* **52,** 1784–1806.

——, 2002: The hydrological cycle in deep-time climate problems. *Nature,* **419,** 191–198.

Rahmstorf, S., 1996: On the freshwater forcing and transport of the Atlantic thermohaline circulation. *Climate Dyn.,* **12,** 799–811.

Stommel, H. M., 1961: Thermohaline convection with two stable regimes of flow. *Tellus,* **13,** 224–230.

——, and G. T. Csanady, 1980: A relation between the T-S curve and global heat and atmospheric water transport. *J. Geophys. Res.,* **85** (C1), 495–501.

Walin, G., 1985: The thermohaline circulation and the control of ice ages. *Palaeogeogr. Palaeoclimatol. Palaeoecol.,* **50,** 323–332.

Wijffels, S. E., R. W. Schmitt, H. L. Bryden, and A. Stigebrandt, 1992: Transport of freshwater by the ocean. *J. Phys. Oceanogr.,* **22,** 155–162.